



HAL
open science

Determination of Heat Release Rate Disturbances in Unconfined Flames Based on Fluctuations in the Travel Time of Ultrasonic Waves

Jingxuan Li, Franck Richecoeur, Thierry Schuller

► **To cite this version:**

Jingxuan Li, Franck Richecoeur, Thierry Schuller. Determination of Heat Release Rate Disturbances in Unconfined Flames Based on Fluctuations in the Travel Time of Ultrasonic Waves. *Combustion Science and Technology*, 2012, 184 (4), pp.533-555. 10.1080/00102202.2011.649323 . hal-00692441

HAL Id: hal-00692441

<https://hal.science/hal-00692441v1>

Submitted on 23 May 2013

HAL is a multi-disciplinary open access archive for the deposit and dissemination of scientific research documents, whether they are published or not. The documents may come from teaching and research institutions in France or abroad, or from public or private research centers.

L'archive ouverte pluridisciplinaire **HAL**, est destinée au dépôt et à la diffusion de documents scientifiques de niveau recherche, publiés ou non, émanant des établissements d'enseignement et de recherche français ou étrangers, des laboratoires publics ou privés.

Determination of heat release rate disturbances in unconfined flames based on fluctuations in the travel time of ultrasonic waves

J.Li^{a,b}, F.Richecoeur^{a,b}, T.Schuller^{a,b,*}

^a*CNRS, UPR 288 Laboratoire d'Energétique Moléculaire et Macroscopique, Combustion (EM2C), Grande Voie des Vignes, 92295 Châtenay-Malabry, France.*

^b*Ecole Centrale Paris, Grande Voie des Vignes, 92295 Châtenay-Malabry, France.*

Abstract

The paper presents a new method to measure heat release rate disturbances from flames when optical access is limited. The technique is based on the determination of the travel time of ultrasonic waves propagating through the flow. The link between heat release rate and sound travel time disturbances depends on the configuration considered. An expression is established here for the case of unconfined premixed flames driven by buoyancy forces associated with the Kelvin-Helmholtz instability formed by the interaction between accelerating hot burned gases and cold ambient air at rest. The system and the principle used for the determination of the sound travel time are then presented and validated under non-reacting conditions. Effects of the main parameters on the precision of this detection technique are examined experimentally. Measurements in reacting conditions are compared to heat release rate data obtained with another technique based on the chemiluminescence

*Corresponding author.

Email address: thierry.schuller@ecp.fr (T.Schuller)

emission. A good agreement is obtained between both signals for the different cases explored demonstrating the sensitivity of the proposed technique.

Keywords: Heat release rate; Chirp excitation method; Ultrasonic waves; Flame flickering; Diagnostic.

1. Introduction

Monitoring and controlling heat release rate disturbances is an important issue in practical combustion chambers because these perturbations are the sources of unsteady thermal stress, direct and indirect combustion noise when entropy waves are accelerated by the mean flow (see for example the recent review by Candel et al. (2009)). They may promote self-sustained thermoacoustic instabilities causing potential severe damages and early aging of components of the combustion chamber (Candel 2002; Lieuwen and Yang 2005). It is therefore necessary to have reliable tools to estimate these disturbances, but direct measurements are not available and techniques generally rely on optical diagnostics.

A widely used technique to estimate heat release rate is to collect the chemiluminescence emission from the flame. Chemiluminescence from hydrocarbon flames results from naturally excited intermediate radicals, such as OH^* , CH^* and C_2^* , formed within the flame front and emitting a photon during the transition to a lower energy state. These radicals are often considered as good markers of heat release rate (Gaydon 1957). Recording the natural emission from the flame is the simplest technique to obtain time-resolved data and is often used to estimate heat release rate perturba-

21 tions by collecting the total emission from the flame (see for example Hurlle
22 et al. (1968); Price et al. (1969); Ducruix et al. (2000)) or by local point
23 measurements (Kojima et al. 2000; Hardalupas and Orain 2004). This has
24 for example been validated in laminar premixed flames submitted to flow
25 modulations in the absence of mixture composition inhomogeneities, where
26 fluctuations in the chemiluminescence emission were shown to be propor-
27 tional to flame surface area disturbances (Schuller et al. 2002). Spectral
28 selection of OH* or CH* emissions is generally preferred for hydrocarbon
29 flames but it is also possible to use other chemiluminescent species, such as
30 C₂* or CO₂* (Samaniengo et al. 1995; Najm et al. 1998; Docquier et al. 2000).
31 In more complex configurations, different additional phenomena modify this
32 relation and effects of the turbulence intensity (Ayoola et al. 2006; Lauer
33 and Sattelmayer 2010), flame strain rate (Hardalupas and Orain 2004; Ay-
34 oola et al. 2006; Nori and Seitzman 2009), flame front curvature (Najm
35 et al. 1998), local mixture composition (Hardalupas and Orain 2004), tem-
36 perature and pressure (Docquier et al. 2000; Higgins et al. 2001; Ikeda et al.
37 2002) must be included to obtain quantitative estimates of the heat release
38 rate. Measurements are then often limited to flame images for qualitative
39 analysis except in a few studies where the signal is calibrated using specific
40 post-processing procedures (see for example Lauer et al. (2011); Palies et al.
41 (2010)). One problem is that the chemiluminescence emission yields an in-
42 formation integrated in the line-of-sight and it is difficult to obtain spatially
43 resolved data. The signal is also more difficult to interpret in non perfectly
44 premixed systems (Balachandran et al. 2005b; Kim et al. 2010).

45

46 One possibility to improve spatial resolution is to use Laser Induced Fluorescence (LIF) by stimulating certain electronic transitions from the radicals
47 present in the flow with a laser sheet intersecting the flame front. OH LIF
48 is widely used since the OH peak mole fraction occurs in the burned gases
49 just behind the reaction zone and the gradients of the fluorescence signal are
50 found to correlate well with the position of the local flame front in turbulent
51 flames (see for example Knikker et al. (2002); Sadanandan et al. (2008)).
52 The CH fluorescence signal is a better tracer of the reaction zone due to
53 its relatively short lifetime and its abundance over a narrow region in the
54 flame zone (Nguyen and Paul 1996; Donbar et al. 2000), even though large
55 deviations with heat release rate were highlighted for diluted flames during
56 transient phenomena (Vagelopoulos and Frank 2005). Time resolved data
57 are more difficult to obtain due to the limited repetition rates and energy de-
58 livered per pulse from the lasers, although OH and CH planar measurements
59 at a few kHz were recently reported to characterize transient phenomena in
60 complex turbulent reacting flows (see for example Tanahashi et al. (2008);
61 Boxx et al. (2009); Stöhr et al. (2011)).
62

63
64 While these techniques enable to locate the flame front, quantitative esti-
65 mates of spatially resolved data for the heat release rate are still challenging.
66 It is generally admitted that the intermediate radical HCO present in the
67 flame front correlates well with heat release rate but the stimulation of an
68 electronic transition with a detectable fluorescence signal raises several diffi-
69 culties (Jeffries et al. 1991). It was shown that the concentration of HCO can
70 however be estimated by the product of the OH and CH₂O radical concen-

71 trations formed around the flame, whose fluorescences are easier to obtain.
72 This has motivated a series of studies based on LIF measurements at different
73 excitation wavelengths to estimate the local distribution of heat release rate
74 in flow configurations of increasing complexity (Najm et al. 1998; Paul and
75 Najm 1998; Fayoux et al. 2005; Balachandran et al. 2005a; Ayoola et al.
76 2006). This type of simultaneous measurements in unsteady flows remain
77 however heavy to implement and require high power well-tuned laser beams
78 at different wavelengths and specific optics.

79

80 The methods briefly presented above are all based on optical detection
81 of radicals present in the flame and are difficult to implement when the op-
82 tical access is limited. The objective of this study is to develop one original
83 solution based on an acoustic method. This new technique relies on deter-
84 mination of the travel time of ultrasonic waves propagating through a flame.

85

86 Flames submitted to acoustic disturbances behave as low-pass filters and
87 are only sensitive to the velocity component of sound waves (Ducruix et al.
88 2003). Low frequency pressure disturbances are transmitted through a flame
89 without distortion. The cut-off frequency of the flame response is reached
90 when the velocity perturbation wavelength is of the order of the flame length
91 $\lambda \sim L$, which is typically limited to about 2 kHz for most typical applica-
92 tions. In the intermediate range of frequencies, sound waves are scattered
93 by the strong jump in density across the flame (Cho 2009) and by turbulent
94 wrinkles which develop along the flame for frequencies ranging from about
95 1 to 20 kHz (Lieuwen 2001). The incoherent scattered sound power first

96 increases exponentially with frequency and then saturates to a certain level
97 when compared to the coherent sound power incident on the flame (Lieuwen
98 et al. 2002). When the wavelength is of the order of the flame thickness, pres-
99 sure perturbations may then strongly interact with the preheat zone $\lambda \sim \delta$
100 and consequently modify the local reaction rate (Peters and Ludford 1983;
101 McIntosh 1991; Ledder and Kapila 1991). This occurs only at very high fre-
102 quencies of the order of 100 kHz for typical hydrocarbon-air flames, except
103 when flames are submitted to high accelerations at very high forcing levels
104 (Durox et al. 1997a; Durox et al. 1998; Wangher et al. 2008).

105

106 Information carried by the scattered field from ultrasonic waves impinging
107 the flow has already been used to analyze vorticity production in turbulent
108 jets and swirling jets (Baerg and Schwarz 1966; Fabrikant 1983; Oljaca et al.
109 1998; Poulain et al. 2004) as well as to detect temperature fluctuations in
110 inert turbulent flows (Contreras and Lund 1990; Elicer-Cortes et al. 2004).
111 In the case of reacting flows, these investigations were limited yet to the
112 examination of the scattered sound field by the flame as a function of the ge-
113 ometric properties of the reaction front and the characteristics of turbulence
114 (Lieuwen et al. 2002; Richecoeur et al. 2009). It is shown in these references
115 that flame front wrinkles induced by turbulence result in Doppler shifted scat-
116 tered waves, the coherent scattered signal being significantly damped com-
117 pared to the incident coherent ultrasonic pressure disturbances, but there has
118 been no attempt yet to use ultrasonic waves to probe reacting flow properties.

119

120 This paper focuses on the use of ultrasonic waves and considers distur-

121 bances of the sound travel time $\Delta t'$ between an emitter and a receiver as an
122 indicator of perturbations in the flame width. This information is then used
123 to reconstruct low frequency heat release rate disturbances \dot{Q}' for unconfined
124 premixed flames driven by buoyancy induced oscillations. This phenomenon
125 called “flickering” is associated with the Kelvin-Helmholtz instability formed
126 by the buoyant interaction between the hot burned gases and cold ambient
127 air (Durox et al. 1997b). It produces small heat release perturbations with
128 typical frequencies around 10 Hz at ground level gravity (Durox et al. 1990;
129 Kostiuk and Cheng 1995) and provides a generic configuration to validate
130 our acoustic methodology for heat release rate reconstruction in the absence
131 of turbulence and external forcing device. Analysis of turbulence effects is
132 out of the scope of the present study and this important topic will be the
133 object of future investigations. Reconstruction of heat release rate for flames
134 submitted to harmonic flowrate modulation has already been undertaken (Li
135 et al. 2011) and the present investigation constitutes the second validation
136 of the technique when gravity effects must be considered.

137

138 The link between the rate of change of the sound travel time $d\Delta t/dt$ for
139 ultrasonic waves crossing the flame and heat release rate fluctuations \dot{Q}' is
140 established in section 2. The experimental configuration is detailed in section
141 3, while the methodology developed to determine the travel time of ultrasonic
142 waves together with the post-processing of the incident and transmitted sig-
143 nals are presented in section 4. This relies on a pulse compression technology
144 used for radar detection. The choice of the type of forcing signal to probe
145 the flow is discussed in section 5. Validation of the acoustic methodology in

146 non-reacting flows is conducted in section 6. Experimental results in react-
147 ing flows are compared to theoretical estimates and data obtained with an
148 optical technique in section 7. Conclusions are drawn in the final section.

149 **2. Model for the sound travel time**

150 The following analysis is restricted to laminar premixed flames charac-
151 terized by a “flickering” of the flame tip induced by buoyancy forces acting
152 on the hot burned gases plume surrounding the flame (Durox et al. 1990;
153 Kostiuk and Cheng 1995). These low frequency oscillations are induced by
154 flow perturbations featuring a large wavelength compared to the flame thick-
155 ness. It is then possible to consider the flame front as a thin interface sepa-
156 rating the reactive mixture from the combustion products. The flame front
157 propagates with the laminar burning velocity S_L and second order effects
158 such as stretch and curvature are neglected in this analysis. Successive ap-
159 proximations are made to obtain an analytical expression of the heat release
160 rate as a function of the sound travel time. These developments offer a sim-
161 ple theoretical framework to analyze effects of the different flow parameters
162 controlling changes in the sound travel time induced by flickering. This is
163 used in the next section to validate the proposed technique by comparisons
164 between predictions and measurements. This analysis is then completed by
165 an independent experimental validation based on an optical technique.

166

Consider the case of a plane sound wave traveling through a homogeneous
gas over a distance L at fixed temperature and composition characterized by

a speed of sound c_u . The propagation time Δt_0 is given by:

$$\Delta t_0 = \frac{L}{c_u} \quad (1)$$

167

168

[Figure 1 about here.]

The burned gases around a flame modify the speed of sound along the acoustic path and consequently change also the sound propagation time. This configuration is represented in Fig. 1 where acoustic waves emitted by a tweeter propagate through three different media corresponding to ambient air, the burned gases and the fresh reactive mixture. In the analysis developed below, ambient air and the unburned gases are characterized by the same speed of sound c_u . This approximation is reasonable for air-combustion systems due to the strong dilution by nitrogen when the reactants are injected at ambient temperature. This situation can be schematically represented by two different media represented in the right part in Fig. 1. The first medium is composed of burned gases characterized by a speed of sound c_b over a length of L_f and the second is filled with ambient air characterized by a speed of sound c_u and a length $L - L_f$. In this case, Eq. (1) is modified and the propagation time Δt of sound waves from the emitter to the receiver now writes:

$$\Delta t = \frac{L - L_f}{c_u} + \int_0^{L_f} \frac{dx}{c_b} \quad (2)$$

By introducing in this expression the sound travel time in the absence of flame Δt_0 which remains constant for a fixed emitter to receiver distance

and taking first order perturbations one obtains:

$$\Delta t' = -\frac{L_f'}{c^*} \quad (3)$$

169 where $c^* = c_u c_b / (c_b - c_u)$ is an equivalent speed of sound. Only disturbances
170 in the acoustic path length L_f are taken into account, fluctuations in temper-
171 ature and composition of the fresh mixture and burned gases are neglected
172 here. This approximation is valid as long as relative perturbations of the
173 equivalent speed of sound remain small $c^{*'} / \bar{c}^* \ll L_f' / \bar{L}_f$, where the super-
174 scripts $(\bar{\cdot})$ and $(\cdot)'$ are used to represent the mean and fluctuating components
175 respectively. This may not be the case in some practical configurations, but
176 it is admitted here.

177

178 For laminar flames stabilized on the rim of a burner, buoyancy effects in-
179 duce a low frequency oscillation of the hot plume without significant change
180 of temperature and composition of the burned gases before the flame tip
181 (Kostiuk and Cheng 1994; Durox et al. 1997b). This results in turn in small
182 perturbations in heat release rate and fluctuations of the burned gases vol-
183 ume. Consequently the length of the acoustic path L_f is also modified. This
184 modification results in a disturbance of the travel time of ultrasonic waves
185 based on Eq. (3).

186

The link between fluctuations in the sound travel time $\Delta t'$ and perturba-
tions in the heat release rate \dot{Q}' must now be established. The main steps
of the derivation are presented below by assuming that the volume of the

burned gases V_b depends on the flame surface area A_f of the conical flame:

$$V_b = \alpha L_f A_f \quad (4)$$

where L_f is the apparent dimension of the burned gases in the line of sight of the emitter and receiver and α denotes a constant coefficient for fixed flow operating conditions and experimental arrangement. Since the flame is anchored at the burner rim, a mass balance between the burner outlet and the flame front yields $v_u A = S_L A_f$, where S_L denotes the laminar burning velocity, v_u represents the flow velocity at the burner outlet and A indicates the section area of the burner outlet. This yields an expression for the hot plume width L_f as a function of the burned gases volume:

$$L_f = \frac{S_L}{\alpha v_u A} V_b \quad (5)$$

In this expression, S_L only depends on the equivalence ratio, v_u is kept constant and α is time independent so that L_f can be substituted in Eq. (3) to yield:

$$\Delta t' = -\frac{S_L}{\alpha v_u A c^*} V_b' \quad (6)$$

187 Fluctuations in the travel time of ultrasonic waves are proportional to fluctu-
 188 ations in the volume of burned gases V_b' . The objective is now to determine
 189 fluctuations of the burned gases volume as a function of heat release rate
 190 disturbances.

191

192 [Figure 2 about here.]

For buoyancy driven oscillations, the flow can be considered isobaric. Using the simplified model presented in Fig. 2, a global energy balance over

the control volume yields:

$$\frac{\gamma p}{\gamma - 1} \left(\frac{\partial V_u}{\partial t} + \frac{\partial V_b}{\partial t} \right) = \dot{m}_u c_p T_u - \dot{m}_b c_p T_b + \dot{Q} \quad (7)$$

where the lateral surface of the control volume in contact with ambient air is supposed impermeable ($\dot{m}_i = 0$) and adiabatic ($\dot{Q}_i = 0$). The ratio of specific heat capacity $\gamma = c_p/c_v$ and ambient pressure p appear on the left side of Eq. (7), while the rate of heat released in the control volume \dot{Q} and the sensible enthalpy fluxes $\dot{m}c_p T$ at the unburned (subscript u) and burned (subscript b) limits are responsible for changes in the unburned V_u and burned V_b volumes. In this expression, T denotes the temperature and \dot{m} represents the mass flow rate. A first order perturbation analysis of Eq. (7) yields at low frequency:

$$\frac{\gamma p}{\gamma - 1} \frac{\partial V_b'}{\partial t} = \dot{Q}' \quad (8)$$

193 where fluctuations in the fresh reactants volume were neglected since $V_u/V_b \approx$
 194 $\rho_b/\rho_u = T_u/T_b \ll 1$. For methane-air flames $T_b/T_u \simeq 5 - 8$ depending on the
 195 mixture equivalence ratio ϕ .

196

Combining Eqs. (6) and (8), one finally finds that heat release rate disturbances induced by buoyancy effects are proportional to the rate of change in the sound travel time between the transmitter and receiver:

$$\dot{Q}' = -\frac{\gamma p}{\gamma - 1} \frac{\alpha v_u A c^*}{S_L} \frac{\partial \Delta t}{\partial t} \quad (9)$$

197 This last relation shows that it is possible to estimate heat release rate per-
 198 turbations induced by flame flickering from fluctuations in the sound propa-
 199 gation time of ultrasonic waves crossing the hot plume of unconfined flames.

200 Heat release rate disturbances are then proportional to the rate of change
201 of the sound travel time $\partial\Delta t/\partial t \propto \dot{Q}'$. The remaining part of this paper is
202 devoted to validation of Eq. (9).

203 **3. Experimental configuration**

204 [Figure 3 about here.]

Experiments are conducted on an axisymmetric burner with a 20 mm outlet nozzle diameter. Laminar premixed methane-air flames are anchored at the burner rim. The flow rates of methane and air are premixed before entering the burner and the equivalence ratio can be modified by adjusting air and methane Bronkhorts massflow controllers. Ultrasonic pulses transmitted to air are generated by a small tweeter placed on one side of the setup, with a working bandwidth from 5 to 50 kHz. The acoustic waves are recorded by two microphones M1 and M2 (B&K, type 4938, working bandwidth 4 Hz - 70 kHz) before and after their passage through (a) a flame or (b) the corresponding jet flow in the absence of combustion. These microphones are aligned so that ultrasonic waves cross on the burner symmetry axis in Fig. 3. A photomultiplier (PM) is also placed on the side of the burner to record the light emission from intermediate radicals present within the flame front. For the laminar premixed flames considered here, it is possible to estimate heat release rate perturbations \dot{Q}' by examining fluctuations in the chemiluminescence intensity I of free radicals OH^* , C_2^* or CH^* present in the reaction zone (Price et al. 1969; Schuller et al. 2002)

$$\dot{Q}' = kI \tag{10}$$

205 The coefficient k is a function of the experimental apparatus and mixture
206 composition. It can be determined by a calibration procedure detailed in
207 section 7.

208 4. Determination of the sound propagation time

209 [Figure 4 about here.]

210 A pulse compression technique is used to determine the propagation time
211 of ultrasonic waves between microphones M1 and M2 (Merrill 2008). Fig-
212 ure 4 presents the block diagram of the transmission and reception systems.
213 A train of pulses, as illustrated in Fig. 5, is synthesized by a wave genera-
214 tor. This signal is amplified and transmitted to space using a tweeter. The
215 ultrasonic waves generated are measured with fixed microphones before and
216 after their passage through the perturbed flow. These sound pressure sig-
217 nals are then amplified, high pass filtered and post-processed to compute the
218 cross-correlation between the incident and transmitted sound waves. Each
219 train of pulses is a chirp signal with a constant amplitude β and a linear
220 frequency modulation over a certain frequency bandwidth B and a time du-
221 ration τ (Fig. 5). This technique enables to obtain a narrow compressed pulse
222 response for the cross-correlation between the incident and transmitted sig-
223 nals with a main peak corresponding to the sought sound travel time Δt .
224 Provided that the repetition time t_r between two successive chirps is large
225 enough, the time resolution of the technique improves as the compression
226 factor $B\tau$ increases (Klauder et al. 1960; Cook and Bernfield 1993; Merrill
227 2008).

228

[Figure 5 about here.]

229

Theoretically, the incident and transmitted signals can be expressed as:

$$S_i(t) = \begin{cases} \beta_i \sin \left(2\pi \left[f_i + \frac{B}{2\tau} t \right] t \right) & 0 \leq t \leq \tau \\ 0 & \text{elsewhere} \end{cases} \quad (11)$$

$$S_t(t) = \begin{cases} \beta_t \sin \left(2\pi \left[f_i + \frac{B}{2\tau} (t - \Delta t) \right] (t - \Delta t) \right) & \Delta t \leq t \leq \tau + \Delta t \\ 0 & \text{elsewhere} \end{cases} \quad (12)$$

The correlation between these two signals is used to obtain a narrow compressed pulse response (Mahafza and Elsherbeni 2004):

$$R_{\text{corr}}(t) = \frac{1}{\tau} \int_{-\infty}^{+\infty} S_t^*(t') S_i(t' - t) dt' \quad (13)$$

230

231

232

233

The sound propagation time Δt is determined by finding the maximum value of the envelope of the cross-correlation response. Examples of ideal generated (Eq. (11)) and transmitted (Eq. (12)) chirps together with the result of the cross-correlation are illustrated in Fig. 6.

234

[Figure 6 about here.]

235

236

237

238

239

240

241

242

Due to the different mechanical and electrical devices in the signal generation and reception, it is not desirable to operate with chirps with a square envelope because of the sudden changes in the signal amplitude at the leading and trailing edges of the sequence. A Hamming window is then applied to the rectangular chirp produced by the signal synthesizer to obtain a smooth transition in amplitude at the beginning and end of the chirp, but the response measured by the different sensors is still distorted as shown in Fig. 7 in the absence of flow between the emitter and receiver.

243

[Figure 7 about here.]

244

[Figure 8 about here.]

245

To improve results, a pre-processing applied to these raw signals is necessary. The technique is the same for the incident and transmitted signals and will only be detailed for the reference microphone M1 in Fig. 8. The raw signal is first filtered with a high pass zero-phase shift filter to eliminate the low frequency background noise induced by the flow and the generation and measurement devices. The filtered result is shown in Fig. 8(a). A digital Butterworth filter with a cut-off frequency $f=100$ Hz featuring an attenuation of less than 3 dB in the pass-band and at least 30 dB in the stop-band was used (Oppenheim and Schaffer 1975). This filtered signal and the signal generated by the synthesizer are processed by the cross-correlation algorithm to locate the leading edge of the chirp. The resulting signal is multiplied by a rectangular box function of duration τ to eliminate the signal outside the chirp as shown in Fig. 8(b). A Hilbert transform is then used to obtain the envelope of the signal, shown in Fig. 8(c). This envelope enables to renormalize the signal presented in Fig. 8(b) and obtain a constant amplitude signal as shown in Fig. 8(d). The pre-processed signals from microphones M1 and M2 are then cross-correlated. The output is again processed by the Hilbert transform to keep only the envelope. The location of the peak of the main lobe yields the propagation time Δt .

264

[Figure 9 about here.]

265

Figure 9 shows an example of the normalized cross-correlation obtained with and without pre-processing. It can be noted that the level reached by the

266

267 side lobes for the pre-processed response is significantly reduced compared to
268 the result obtained without pre-processing. The resolution of the technique
269 is indicated by the width of the main peak calculated at the level 0.5. The
270 pre-processing clearly improves the result.

271 5. Parameters optimization for the chirp generation

272 [Table 1 about here.]

273 Different tests were conducted in the absence of flow and flame to opti-
274 mize the technique for the generation and detection of the chirp ultrasonic
275 signals. The influence of the frequency bandwidth B , initial frequency f_i ,
276 chirp duration τ and chirp repetition rate t_r on the precision of the mea-
277 sured sound travel time Δt was analyzed in this section. To avoid mixing
278 different neighbor transmitted signals, the duration between two pulses $t_r - \tau$
279 must be larger than the fluctuations of propagation time Δt . It was checked
280 in this case that results were independent on the repetition rate t_r . The
281 range explored for the values of the three remaining parameters is synthe-
282 sized in Tab. 1. In this table, the carrier frequency $f_0 = f_i + B/2$ is indicated
283 instead of f_i to examine effects of the initial frequency. The influence of each
284 parameter was studied separately by keeping the two others fixed. In these
285 experiments, the signals from the microphones were sampled at a frequency
286 $f_s = 2^{21}$ Hz over a duration 0.2 s and measurements were repeated 100 times
287 for each case explored to obtain the confidence interval of the samples.

288 [Figure 10 about here.]

289 The measured sound travel times are plotted as a function of the fre-
290 quency bandwidth B , pulse duration τ and carrier frequency f_0 respectively
291 in Fig. 10. In these plots, error bars correspond to the maximal deviation
292 over 100 repetitions and the black disks denote the mean value. It can be
293 noted that an increase in the frequency bandwidth B or pulse-width dura-
294 tion τ greatly improves the precision in Fig. 10(a) and (b), but the choice of
295 the pulse-width duration is limited when time resolved data are needed. For
296 example, to obtain time resolved records with a sampling rate of 500 Hz, τ
297 has to be less than 2 ms. Theoretically, the carrier frequency f_0 or initial
298 frequency f_i has no effect on the precision (Merrill 2008). Figure 10(c) shows
299 however that results feature some scatter depending on f_0 . This phenomenon
300 is again induced by the different mechanical and electronic responses of the
301 transmitter and receiver devices. In the remaining experiments, the parame-
302 ters chosen for the chirp generation were fixed to the optimal values indicated
303 in Tab. 2.

304 [Table 2 about here.]

305 6. Validation in the absence of flame

306 The transmission of sound waves between microphones M1 and M2 under
307 non-reacting conditions was investigated. Experiments were conducted for
308 three different cases, (a) without burner, (b) with the burner between the
309 two microphones but in the absence of flow, and (c) for a non-reacting jet
310 flow (Fig. 3). The Reynolds number based on the flow velocity and nozzle
311 diameter $Re = 2900$ corresponds to a laminar jet with a flow velocity typical
312 of the reacting conditions explored in the next section. Parameters used to

313 generate the chirp are listed in Tab. 2. Microphones signals were sampled
314 here at a frequency $f_s = 2^{21}$ Hz during a period of 0.2 s. This duration is
315 long enough to collect 80 transmitted chirps for each record.

316

317 [Figure 11 about here.]

318 By modifying the horizontal position of M2 (Fig. 3), it is possible to de-
319 termine the evolution of the travel time of ultrasonic waves Δt_0 as a function
320 of the distance L between the two microphones. In these experiments, the
321 horizontal distance between the two microphones was increased by steps of
322 5 mm to record the different sets of data. The evolution of the difference
323 $\Delta(\Delta t_0) = \Delta t_0(L) - \Delta t_0(L_0)$ between measurements of the sound travel time
324 recorded for two distances L and L_0 between microphones M1 and M2 is
325 plotted in Fig. 11 as a function of the distance $\Delta L = L - L_0$, where the ref-
326 erence distance corresponds to $L_0 = 300$ mm. The difference in sound travel
327 time $\Delta(\Delta t_0)$ increases linearly with ΔL for all cases explored. All data col-
328 lapse on the same line indicating that there is no scattering effects due to
329 the presence of the burner or laminar jet. The slope $1/c_0$ indeed fits with
330 predictions from Eq. (1), where $c_0 = 348$ m.s⁻¹ is the speed of the sound in
331 ambient air. This setup and the methodology developed can now be used to
332 examine perturbations in the sound travel time induced by the presence of
333 the flame between the two microphones.

334 7. Validation with flame

335 [Figure 12 about here.]

336 Laminar premixed conical flames are stabilized on the burner rim. As
337 already discussed in the previous sections, while the flow is steady, the tip of
338 the conical flame features a small regular oscillation called flickering caused
339 by the unstable interface between the burned gases and ambient air (Fig. 12,
340 left image). It is also known that a cylindrical tube on the top of the flame
341 stabilizes the flow of the burned gases and the flickering phenomenon is at-
342 tenuated (Kizirnis et al. 1984; Linteris and Rafferty 2008). This is illustrated
343 in the right image in Fig. 12. Flickering features typical frequencies around
344 10 – 20 Hz (Kostiuk and Cheng 1994; Durox et al. 1997b). This motion
345 generates in turn small low frequency heat release rate perturbations that
346 can be identified by measuring fluctuations in the light emission intensity I
347 recorded by the PM or by determining fluctuations in the sound travel time
348 Δt with the microphones M1 and M2.

349 [Figure 13 about here.]

Measurements are shown for a lean methane-air flame with a bulk velocity $v_u=1.5 \text{ m.s}^{-1}$ and equivalence ratio $\phi = 0.9$ with and without a quartz tube on the top of the flame. Signals are recorded here with the same sampling frequency $f_s = 2^{11} \text{ Hz}$ but over a longer sampling time 1.5 s than in the experiments in the absence of combustion. The left graph in Fig. 13 shows that the light intensity $I(t)$ and sound travel time Δt both feature a periodic motion. Power spectral analysis based on the data collected with the PM and the microphones show that the main peak in both cases corresponds to the oscillation frequency $f = 16 \pm 1 \text{ Hz}$. These measurements are in agreement with the flickering frequency deduced from the correlation of (Kostiuk and

Cheng 1994):

$$\frac{f^2 D}{g\xi(\xi - 1)} = 0.00028 \left(\frac{v_u D}{\xi\nu} \right)^{2/3} \quad (14)$$

350

351 By taking $D = 20$ mm for the diameter of the burner outlet, $g = 9.8 \text{ m.s}^{-2}$
352 for the gravitational acceleration, $\xi = T_b/T_u = 7$ for the volumetric expansion
353 ratio and $\nu = 1.5 \times 10^{-5} \text{ m}^2.\text{s}^{-1}$ for the kinematic viscosity in the fresh
354 reactants at room temperature, one also finds $f = 16$ Hz. This confirms that
355 the two previous techniques highlight the same unsteady behavior induced
356 by flame flickering. Results presented on the right in Fig. 13 clearly demon-
357 strate that fluctuations in the light intensity I and travel time of ultrasonic
358 waves Δt vanish when the quartz tube is used.

359

360 [Figure 14 about here.]

Fluctuations in the chemiluminescence emission intensity I and disturbances in the sound travel time Δt result both from heat release rate perturbations. The link between these quantities is obtained by plotting the evolution of the mean value of the light intensity \bar{I} as a function of the flow velocity v_u at the burner outlet. Results are presented in Fig. 14 for four flames featuring different equivalence ratios $\phi = 0.85, 0.90, 0.95$ and 1.00 . The evolution is linear $\bar{I} = \epsilon v_u$, where the coefficient ϵ depends on the equivalence ratio of the combustible mixture. It is then possible to obtain an expression for the coefficient k appearing in Eq. (10) linking the heat release rate \bar{Q} and the chemiluminescence intensity \bar{I} :

$$k = \frac{\bar{Q}}{\bar{I}} = \frac{\bar{Q}}{\epsilon v_u} = \frac{\rho_u \Delta q A}{\epsilon} \quad (15)$$

where ρ_u is the unburned mixture density, A the cross section area at the burner outlet and Δq the heating value per unit mass of reactive mixture. In this expression, it is assumed that all the mixture is burned. Combining Eqs. (9) and (15), the following relation between perturbations in chemiluminescence intensity I and sound travel time Δt can be derived:

$$\frac{d\Delta t}{dt} = \Xi I' \quad \text{where} \quad \Xi = -\frac{(\gamma - 1) S_L \Delta q}{\alpha \epsilon v_u c_u^2 c^*} \frac{1}{c^*} \quad (16)$$

361 For a fixed mixture composition and flow velocity, fluctuations in the flame
 362 emission are proportional to the rate of change of the sound travel time of
 363 acoustic waves crossing the flame.

364

365 [Table 3 about here.]

366 In this study, conical flames featuring a regular flickering of the tip were
 367 found for operating conditions corresponding to equivalence ratios $\phi=[0.85$
 368 $1.50]$. It was not possible to stabilize flames leaner than $\phi=0.85$ that blow-
 369 off. The rich limit $\phi=1.50$ corresponds to a situation where the conical flame
 370 tip opens and the flickering phenomenon disappears. One difficulty with fuel
 371 rich operating conditions ($\phi \geq 1$) is that a diffusion flame surrounds the pre-
 372 mixed conical flame stabilized in the center region, where the remaining fuel
 373 is burned. In these conditions, techniques based on analysis of the chemilumi-
 374 nescence emission do not reproduce heat release rate disturbances (Lauer and
 375 Sattelmayer 2010). This study was thus limited to fuel lean flames ($\phi \leq 1$).
 376 Measurements of $d\Delta t/dt$ and I' were conducted for lean premixed methane-
 377 air flames featuring different inlet flow velocities ranging from $v_u = 0.84$ to

378 1.68 m.s^{-1} and equivalence ratios ϕ varying from 0.85 to 1.00. Parameters
 379 fixed for the chirp generation are indicated in Tab. 2. Acoustic measurements
 380 were sampled at a frequency equal to 400 Hz corresponding to a repetition
 381 time $t_r = 2.5 \text{ ms}$. The resulting signal for $\Delta t'$ was then filtered by a low-pass
 382 zero-phase shift filter with a cut-off frequency equal to 40 Hz. The PM signal
 383 was sampled at a frequency of 8192 Hz during a period of 1.5 s and is filtered
 384 with the same low pass filter. Comparisons between the two measurement
 385 techniques are presented in Fig. 15 for the six cases listed in Tab. 3. The
 386 opposite signal $-I'$ is plotted in this figure because the proportionality coef-
 387 ficient Ξ between I' and $d\Delta t'/dt$ given by Eq. (16) is negative. Signals were
 388 also rescaled in this figure to obtain comparable oscillations levels. The two
 389 signals $d\Delta t'/dt$ and $-I'$ match well in phase and relative amplitude for all
 390 cases, clearly demonstrating that the rate of change of the sound travel time
 391 of ultrasonic waves is proportional to fluctuations in light intensity emission:
 392 $d\Delta t'/dt \propto I'$.

393 [Figure 15 about here.]

394 [Figure 16 about here.]

395 Instead of plotting the signals $d\Delta t'/dt$ and I' as a function of time like
 396 in Fig. 15, it is also interesting to plot $d\Delta t'/dt$ as a function of I' for the
 397 different operating conditions explored. One example is presented in Fig. 16
 398 for the case C2 (see Tab. 3). The value of the coefficient Ξ appearing in
 399 Eq. (16) can then be determined by a linear regression. These values and the
 400 corresponding regression coefficients r^2 are indicated in Tab. 3 and confirm
 401 the linear link between $d\Delta t'/dt$ and I' for all cases explored. Data determined

402 experimentally can also be compared to predictions using values indicated
403 in Tab. 4 to estimate the coefficient Ξ appearing in Eq. (16). Predictions
404 are plotted in Fig. 17 and are compared to measurements for two different
405 equivalence ratios $\phi = 0.85$ and $\phi = 1.00$ as a function of the nozzle outlet
406 flow velocity v_u . The distributions of experimental results match well again
407 predictions confirming the validity of Eq. (16) and the possibility to detect
408 heat release rate fluctuations by measuring perturbations in the transmission
409 time of ultrasonic waves crossing flames.

410 [Table 4 about here.]

411 [Figure 17 about here.]

412 8. Conclusion

413 A new technique was presented to detect small heat release rate distur-
414 bances in premixed flames submitted to low frequency instabilities driven by
415 buoyancy forces when the optical access is limited. This technique is based on
416 the determination of the travel time of ultrasonic waves transmitted through
417 the flames. An experimental validation of the proposed technique was con-
418 ducted on a generic configuration with a tweeter to produce the ultrasonic
419 waves and two microphones to record the incident and transmitted signals
420 through different laminar flames. An analytical relation was derived linking
421 sound travel time and heat release rate disturbances. Time resolved measure-
422 ments obtained with the acoustic methodology were compared with optical
423 data based on records of the chemiluminescence emission from the flames. A
424 good agreement was obtained for the different cases explored demonstrating

425 that the transmission of ultrasonic waves can effectively be used to estimate
426 heat release rate disturbances. It was also shown that the proposed technique
427 is very sensitive to small disturbances in heat release rate. These results are
428 encouraging and motivate further development of this technique to investi-
429 gate heat release rate disturbances in more complex configurations.

430 **Aknowledgement**

431 Jingxuan Li is supported by a doctoral fellowship from China Scholarship
432 Council, Project 111, Grant No. B08009. The authors wish to thank Dr.
433 Daniel Durox for helpful discussion about buoyancy effects and assistances
434 with color Schlieren technique.

435 **References**

- 436 Ayoola, B., R. Balachandran, J. Frank, E. Mastorakos, and C. Kaminski
437 (2006). Spatially resolved heat release rate measurements in turbulent
438 premixed flames. *Combust. Flame* 144(1-2), 1–16.
- 439 Baerg, W. and W. Schwarz (1966). Measurements of the scattering of
440 sound from turbulence. *J. Acoust. Soc. Am.* 39(6), 1125–1132.
- 441 Balachandran, R., B. Ayoola, C. Kaminski, A. Dowling, and E. Mastorakos
442 (2005a). Experimental investigation of the nonlinear response of tur-
443 bulent premixed flames to imposed inlet velocity oscillations. *Combust.*
444 *Flame* 143(1-2), 37–55.
- 445 Balachandran, R., A. P. Dowling, and E. Mastorakos (2005b, April). Re-
446 sponse of turbulent premixed flames subjected to inlet velocity and

- 447 equivalence ratio perturbations. Louvain-la-Neuve. European Combustion Meeting.
448
- 449 Boxx, I., M. Stöhr, C. Carter, and W. Meier (2009). Sustained multi-kHz
450 flamefront and 3-component velocity-field measurements for the study
451 of turbulent flames. *Appl. Phys. B-Lasers Opt.* 95(1), 23–29.
- 452 Candel, S. (2002). Combustion dynamics and control: Progress and chal-
453 lenges. *Proc. Combust. Inst.* 29(1), 1–28.
- 454 Candel, S., D. Durox, S. Ducruix, A.-L. Birbaud, N. Noiray, and
455 T. Schuller (2009). Flame dynamics and combustion noise: progress
456 and challenges. *Int. J. Aeroacoustics* 8(1), 1–56.
- 457 Cho, J. (2009). Analysis of low-frequency wave scattering by turbulent
458 premixed flame. *J. Fluid Mech.* 634, 137–164.
- 459 Contreras, H. and F. Lund (1990). Ultrasound as a probe of turbulence.
460 II. Temperature inhomogeneities. *Phys. Lett. A* 149(2-3), 127–130.
- 461 Cook, C. E. and M. Bernfield (1993). *Radar Signals: An Introduction to*
462 *Theory and Application*. Artech House Publishers, London.
- 463 Docquier, N., S. Belhafaoui, F. Lacas, N. Darabiha, and C. Rolon
464 (2000). Experimental and numerical study of chemiluminescence in
465 methane/air high-pressure flames for active control applications. *Proc.*
466 *Combust. Inst.* 28(2), 1765–1774.
- 467 Donbar, J., J. Driscoll, and C. Carter (2000). Reaction zone structure in
468 turbulent nonpremixed jet flames—from CH-OH PLIF images. *Combust.*
469 *Flame* 122(1-2), 1–19.

- 470 Ducruix, S., D. Durox, and S. Candel (2000). Theoretical and experimental
471 determinations of the transfer function of a laminar premixed flame.
472 *Proc. Combust. Inst.* 28(1), 765–773.
- 473 Ducruix, S., T. Schuller, D. Durox, and S. Candel (2003). Combustion dy-
474 namics and instabilities: Elementary coupling and driving mechanisms.
475 *J. Propuls. Power* 19(5), 722–734.
- 476 Durox, D., F. Baillot, P. Scoufflaire, and R. Prud’homme (1990). Some
477 effects of gravity on the behaviour of premixed flames. *Combust.*
478 *Flame* 82(1), 66–74.
- 479 Durox, D., F. Baillot, G. Searby, and L. Boyer (1997a). On the shape
480 of flames under strong acoustic forcing: a mean flow controlled by an
481 oscillating flow. *J. Fluid Mech.* 350, 295–310.
- 482 Durox, D., S. Ducruix, and F. Baillot (1998). Strong acoustic forcing on
483 conical premixed flames. *Proc. Combust. Inst.* 27(1), 883–889.
- 484 Durox, D., T. Yuan, and E. Villermaux (1997b). The effect of buoyancy on
485 flickering in diffusion flames. *Combust. Sci. and Tech.* 124(1-6), 277–
486 294.
- 487 Elicer-Cortes, J. C., R. Contreras, D. Boyer, M. Pavageau, and R. H. Her-
488 nandez (2004). Temperature spectra from a turbulent thermal plume
489 by ultrasound scattering. *Exp. Therm. Fluid Sci.* 28(8), 803–813.
- 490 Fabrikant, A. (1983). Sound scattering by vortex flows. *Sov. Phys.*
491 *Acoust.* 29, 152–154.
- 492 Fayoux, A., K. Zäringher, O. Gicquel, and J. Rolon (2005). Experimental
493 and numerical determination of heat release in counterflow premixed

- 494 laminar flames. *Proc. Combust. Inst.* 30(1), 251–257.
- 495 Gaydon, A. G. (1957). *The spectroscopy of flames*. Wiley, New York.
- 496 Hardalupas, Y. and M. Orain (2004). Local measurements of the time-
497 dependent heat release rate and equivalence ratio using chemilumines-
498 cent emission from a flame. *Combust. Flame* 139(3), 188–207.
- 499 Higgins, B., M. Q. McQuay, F. Lacas, and S. Candel (2001). An exper-
500 imental study on the effect of pressure and strain rate on CH chemi-
501 luminescence of premixed fuel-lean methane/air flames. *Fuel* 80(11),
502 1583–1591.
- 503 Hurle, I. R., R. B. Price, T. M. Sugden, and A. Thomas (1968, March).
504 Sound Emission from Open Turbulent Premixed Flames. *Proc. Roy.*
505 *Soc. London Ser. A* 303, 409–427.
- 506 Ikeda, Y., J. Kojima, and H. Hashimoto (2002). Local chemilumines-
507 cence spectra measurements in a high-pressure laminar methane/air
508 premixed flame. *Proc. Combust. Inst.* 29(2), 1495–1501.
- 509 Jeffries, J. B., D. R. Crosley, I. J. Wysong, and G. P. Smith (1991). Laser-
510 induced fluorescence detection of HCO in a low-pressure flame. *Proc.*
511 *Combust. Inst.* 23(1), 1847–1854.
- 512 Kim, K., J. Lee, B. Quay, and D. Santavicca (2010). Response of partially
513 premixed flames to acoustic velocity and equivalence ratio perturba-
514 tions. *Combust. Flame* 157(9), 1731–1744.
- 515 Kizirnis, S. W., R. J. Brecha, B. N. Ganguly, L. P. Goss, , and R. Gupta
516 (1984). Hydroxyl (OH) distributions and temperature profiles in a pre-
517 mixed propane flame obtained by laser deflection techniques. *Appl.*

518 *Opt. 23*, 3873–3880.

519 Klauder, J., A. C. Price, S. Darlington, and W. J. Albersheim (1960,
520 July). The theory and design of chirp radars. *Bell Sys. Tech. J.* *39*(4),
521 745–808.

522 Knikker, R., D. Veynante, and C. Meneveau (2002). A priori testing of a
523 similarity model for large eddysimulations of turbulent premixed com-
524 bustion. *Proc. Combust. Inst.* *29*(2), 2105–2111.

525 Kojima, J., Y. Ikeda, and T. Nakajima (2000). Spatially resolved measure-
526 ment of OH*, CH*, and C2* chemiluminescence in the reaction zone
527 of laminar methane/air premixed flames. *Proc. Combust. Inst.* *28*(2),
528 1757–1764.

529 Kostiuk, L. W. and R. K. Cheng (1994). Imaging of premixed flames in
530 microgravity. *Exp. Fluids* *18*(1-2), 59–68.

531 Kostiuk, L. W. and R. K. Cheng (1995). The coupling of conical wrinkled
532 laminar flames with gravity. *Combust. Flame* *103*(1-2), 27–40.

533 Lauer, M. and T. Sattelmayer (2010). On the adequacy of chemilumines-
534 cence as a measure for heat release in turbulent flames with mixture
535 gradients. *J. Eng. Gas Turb. Power* *132*, 061502 (8 pages).

536 Lauer, M., M. Zellhuber, C. Aul, and T. Sattelmayer (2011). Determina-
537 tion of the Heat Release Distribution in Turbulent Flames by a Model
538 Based Correction of OH* Chemiluminescence. In *Proceedings of the*
539 *ASME Turbo Expo 2011*, Number GT2011-45105.

540 Ledder, G. and A. Kapila (1991). The response of premixed flames to
541 pressure perturbations. *Combust. Sci. Tech.* *76*(1-3), 21–44.

- 542 Li, J., F. Richecoeur, Y. Huang, and T. Schuller (2011). An acoustic
543 methodology to measure heat release rate fluctuations from unsteady
544 laminar flames. In *Proceedings of the ASME Turbo Expo 2011*, Number
545 GT2011-46431 (10 pages).
- 546 Lieuwen, T. (2001). Theory of high frequency acoustic wave scattering by
547 turbulent flames. *Combust. Flame* 126(1-2), 1489–1505.
- 548 Lieuwen, T., R. Rajaram, Y. Neumeier, and S. Nair (2002). Measurements
549 of incoherent acoustic wave scattering from turbulent premixed flames.
550 *Proc. Combust. Inst.* 29(2), 1809–1815.
- 551 Lieuwen, T. C. and V. Yang (Eds.) (2005). *Combustion instabilities in*
552 *gas turbines, Operational experience, Fundamental mechanisms, and*
553 *Modeling*, Volume 210 of *Progress in Astronautics and Aeronautics*.
554 AIAA, Inc.
- 555 Linteris, G. and I. Rafferty (2008). Flame size, heat release, and smoke
556 points in materials flammability. *Fire Safety J.* 43(6), 442–450.
- 557 Mahafza, B. R. and A. Z. Elsherbeni (2004). *Matlab Simulations for Radar*
558 *Systems Design*. Chapman and Hall, New York.
- 559 McIntosh, A. C. (1991). Pressure disturbances of different length scales
560 interacting with conventional flames. *Combust. Sci. Tech.* 75(4-6), 287–
561 309.
- 562 Merrill, S. (2008). *Radar Handbook, 3rd Edition*. McGraw-Hill, New York.
- 563 Najm, H., P. Paul, C. Mueller, and P. Wyckoff (1998). On the adequacy
564 of certain experimental observables as measurements of flame burning
565 rate. *Combust. Flame* 113(3), 312–332.

- 566 Nguyen, Q.-V. and P. H. Paul (1996). The time evolution of a vortex-flame
567 interaction observed via planar imaging of ch and oh. *Proc. Combust.*
568 *Inst.* 26(1), 357–364.
- 569 Nori, V. N. and J. M. Seitzman (2009). CH* chemiluminescence modeling
570 for combustion diagnostics. *Proc. Combust. Inst.* 32(1), 895–903.
- 571 Oljaca, M., A. Glezer, M. Baffico, and F. Lund (1998). Ultrasound scat-
572 tering by a swirling jet. *Phys. Fluids* 10(4), 886–898.
- 573 Oppenheim, V. and R. Schafer (1975). *Digital signal processing*. Prentice-
574 Hall.
- 575 Palies, P., D. Durox, T. Schuller, and S. Candel (2010). The combined
576 dynamics of swirler and turbulent premixed swirling flames. *Combust.*
577 *Flame* 157(9), 1698–1717.
- 578 Paul, P. and H. Najm (1998). Planar laser-induced fluorescence imaging
579 of flame heat release rate. *Proc. Combust. Inst.* 27(1), 43–50.
- 580 Peters, N. and G. Ludford (1983). The effect of pressure variations on
581 premixed flames. *Combust. Sci. Tech.* 34(1-6), 331–344.
- 582 Poulain, C., N. Mazellier, P. Gervais, Y. Gagne, and C. Baudet (2004).
583 Spectral vorticity and lagrangian velocity measurements in turbulent
584 jets. *Flow Turbul. Combust.* 72(2-4), 245–271.
- 585 Price, R., I. Hurle, and T. Sugden (1969). Optical studies of the generation
586 of noise in turbulent flames. *Proc. Combust. Inst.* 12(1), 1093–1102.
- 587 Richecoeur, F., S. Ducruix, P. Scoufflaire, and S. Candel (2009). Effect
588 of temperature fluctuations on high frequency acoustic coupling. *Proc.*

- 589 *Combust. Inst.* 32(2), 1663–1670.
- 590 Sadanandan, R., M. Stöhr, and W. Meier (2008). Simultaneous OH-PLIF
591 and PIV measurements in a gas turbine model combustor. *Appl. Phys.*
592 *B-Lasers Opt.* 90(3-4), 609–618.
- 593 Samaniengo, J., F. Egolfopoulos, and C. Bowman (1995). CO₂* chemi-
594 luminescence in premixed flames. *Combust. Sci. and Tech.* 109(1-6),
595 183–203.
- 596 Schuller, T., D. Durox, and S. Candel (2002). Dynamics of and noise
597 radiated by a perturbed impinging premixed jet flame. *Combust.*
598 *Flame* 128(1-2), 88–110.
- 599 Stöhr, M., I. Boxx, C. Carter, and W. Meier (2011). Dynamics of lean
600 blowout of a swirl-stabilized flame in a gas turbine model combustor.
601 *Proc. Combust. Inst.* 33(2), 2953–2960.
- 602 Tanahashi, M., S. Taka, M. Shimura, and T. Miyauchi (2008). CH double-
603 pulsed PLIF measurement in turbulent premixed flame. *Exp. Flu-*
604 *ids* 45(2), 323–332.
- 605 Vagelopoulos, C. M. and J. H. Frank (2005). An experimental and numeri-
606 cal study on the adequacy of ch as a flame marker in premixed methane
607 flames. *Proc. Combust. Inst.* 30(1), 241–249.
- 608 Wangher, A., G. Searby, and J. Quinard (2008). Experimental investi-
609 gation of the unsteady response of premixed flame fronts to acoustic
610 pressure waves. *Combust. Flame* 154(1-2), 310–318.

611 **List of Figures**

612 1 Schematic of the configuration investigated. A sound wave
613 generated by an ultrasonic emitter propagates through ambi-
614 ent air, the burned gases formed around a flame before reach-
615 ing a receiver. The distance between the emitter and receiver
616 is L . Waves propagates through the burned gases over a dis-
617 tance L_f 35

618 2 Control volume divided in two parts by the flame: unburned
619 gases (volume V_u and mass flowrate \dot{m}_u) and burned gases
620 (volume V_b and mass flowrate \dot{m}_b). 36

621 3 Schematic view of the experimental setup. 37

622 4 Block diagram for the pulse compression generation and de-
623 tection measurement chains. 38

624 5 Schematic of a train of chirp signals. f_i : chirp initial fre-
625 quency; τ : chirp duration; t_r : repetition time; B : chirp fre-
626 quency bandwidth. 39

627 6 Examples of the ideal incident signal (a) and transmitted sig-
628 nal (b) together with their cross-correlation (c). 40

629 7 Example of chirp record in the absence of flow, (a) signal from
630 the signal synthesizer output, (b) signal recorded by M1, (c)
631 signal recorded by M2. 41

632 8 Pre-processing of signal measured by M1. (a) high pass filtered
633 signal; (b) output of the multiplication between the filtered
634 signal and the rectangular box function; (c) envelope of the
635 signal; (d) normalized signal. 42

636 9 Comparison of the cross-correlations with (black line) and
637 without pre-processing (gray line). 43

638 10 Effects of the chirp parameters on the determination of the
639 sound travel time Δt . See Tab. 1 for values of the remain-
640 ing parameters. The distance between the transmitter and
641 receiver is $L = 300$ mm. The speed of sound at ambient con-
642 ditions is $c_o = 348$ m.s⁻¹. Theoretically, the sound travel time
643 is $\Delta t_{th} = 860$ μ s in this case. 44

644	11	Evolution of the sound travel time difference $\Delta(\Delta t_0) = \Delta t_0(L) - \Delta t_0(L_0)$ with the distance $\Delta L = L - L_0$. The solid line indicates theoretical predictions deduced from Eq. (1). Markers denote measures in the absence of burner (\square), with burner (+), and for a non-reacting jet flow (\star).	45
645			
646			
647			
648			
649	12	Color Schlieren images of a methane-air premixed flame ($\phi = 0.90$, $v_u = 1.50$ m.s ⁻¹) with and without quartz tube on the top of the flame.	46
650			
651			
652	13	Light emission (top) and sound propagation time (bottom) across a methane-air premixed flame ($\phi = 0.90$, $v_u = 1.50$ m.s ⁻¹) with and without flickering.	47
653			
654			
655	14	Evolution of the mean flame emission intensity \bar{I} as a function of the flow velocity v_u for different equivalence ratios ϕ	48
656			
657	15	Simultaneous records of chemiluminescence intensity perturbations $-I'$ (solid line) and disturbances in the rate of change of the sound travel $d\Delta t/dt$ (+).	49
658			
659			
660	16	Plot of the rate of change of travel time of ultrasonic waves $d\Delta t/dt$ versus light intensity fluctuations of the flames I' . Flame C2: $\phi = 0.85$ and $v_u = 1.24$ m.s ⁻¹	50
661			
662			
663	17	Comparison between measurements and predictions (solid line) for the coefficient Ξ for two equivalence ratios $\phi = 0.85$ (∇) and $\phi = 1.0$ (\circ) as function of the flow velocity v_u	51
664			
665			

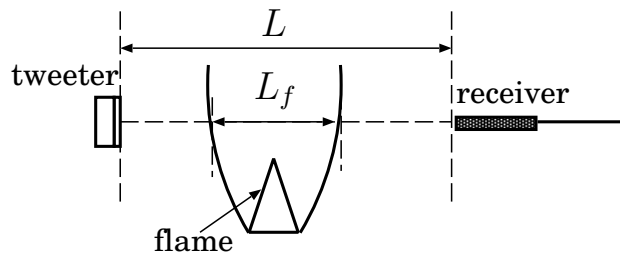


Figure 1: Schematic of the configuration investigated. A sound wave generated by an ultrasonic emitter propagates through ambient air, the burned gases formed around a flame before reaching a receiver. The distance between the emitter and receiver is L . Waves propagates through the burned gases over a distance L_f .

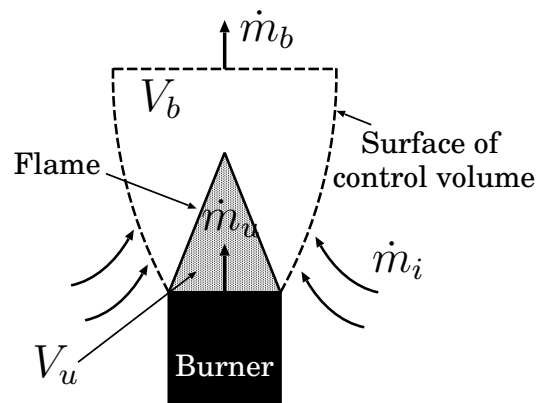


Figure 2: Control volume divided in two parts by the flame: unburned gases (volume V_u and mass flowrate \dot{m}_u) and burned gases (volume V_b and mass flowrate \dot{m}_b).

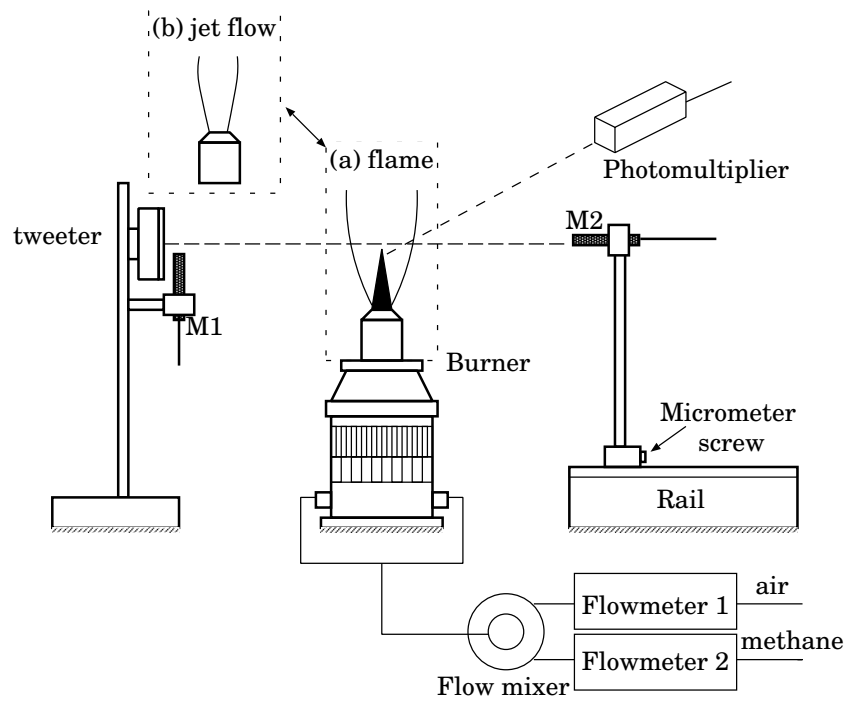


Figure 3: Schematic view of the experimental setup.

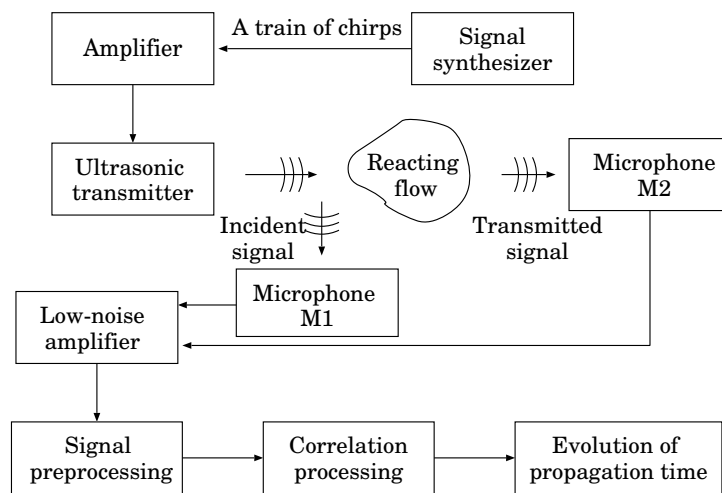


Figure 4: Block diagram for the pulse compression generation and detection measurement chains.

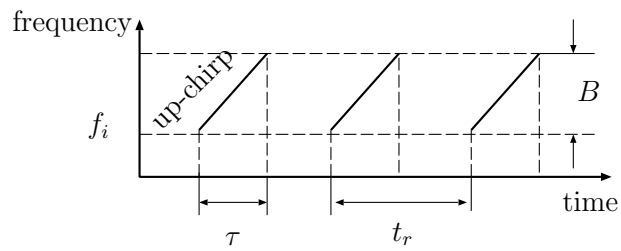
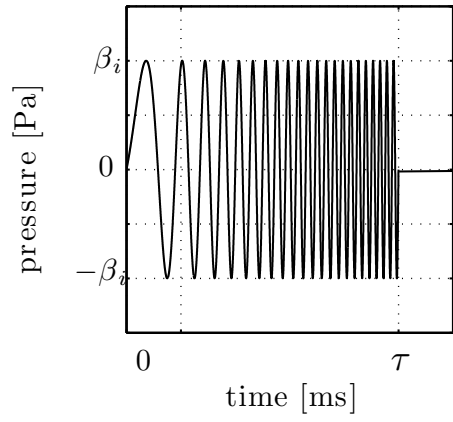
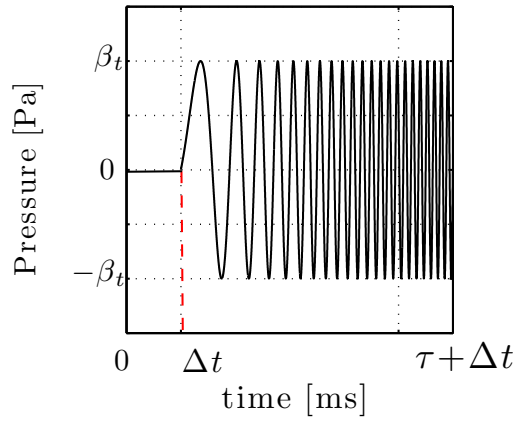


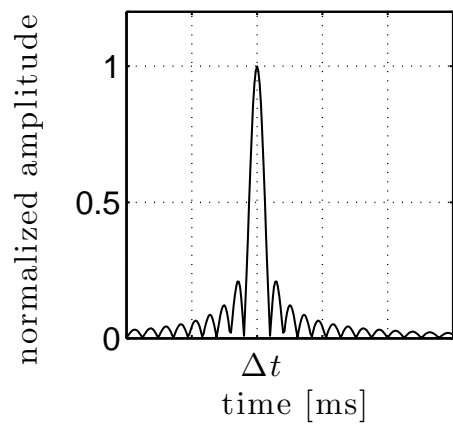
Figure 5: Schematic of a train of chirp signals. f_i : chirp initial frequency; τ : chirp duration; t_r : repetition time; B : chirp frequency bandwidth.



(a)



(b)



(c)

Figure 6: Examples of the ideal incident signal (a) and transmitted signal (b) together with their cross-correlation (c).

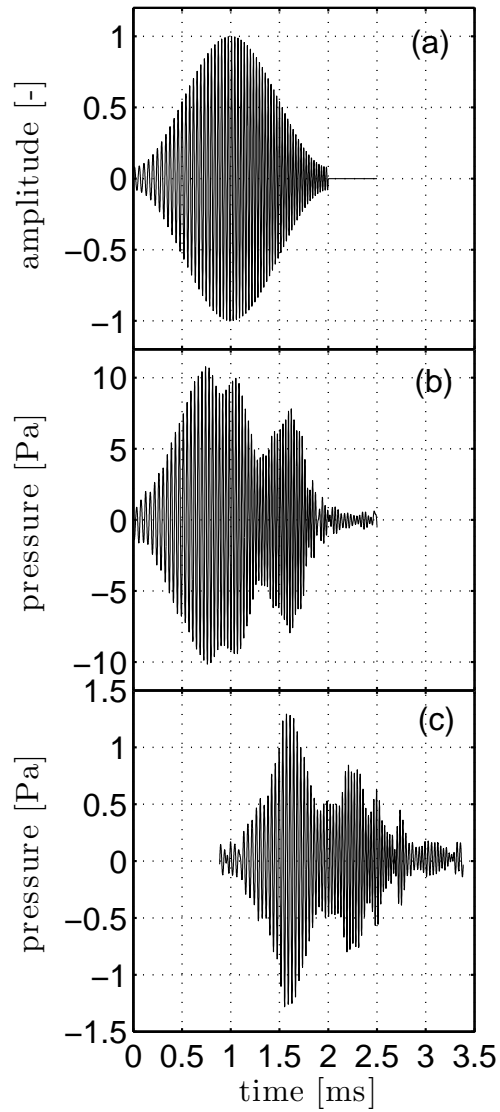


Figure 7: Example of chirp record in the absence of flow, (a) signal from the signal synthesizer output, (b) signal recorded by M1, (c) signal recorded by M2.

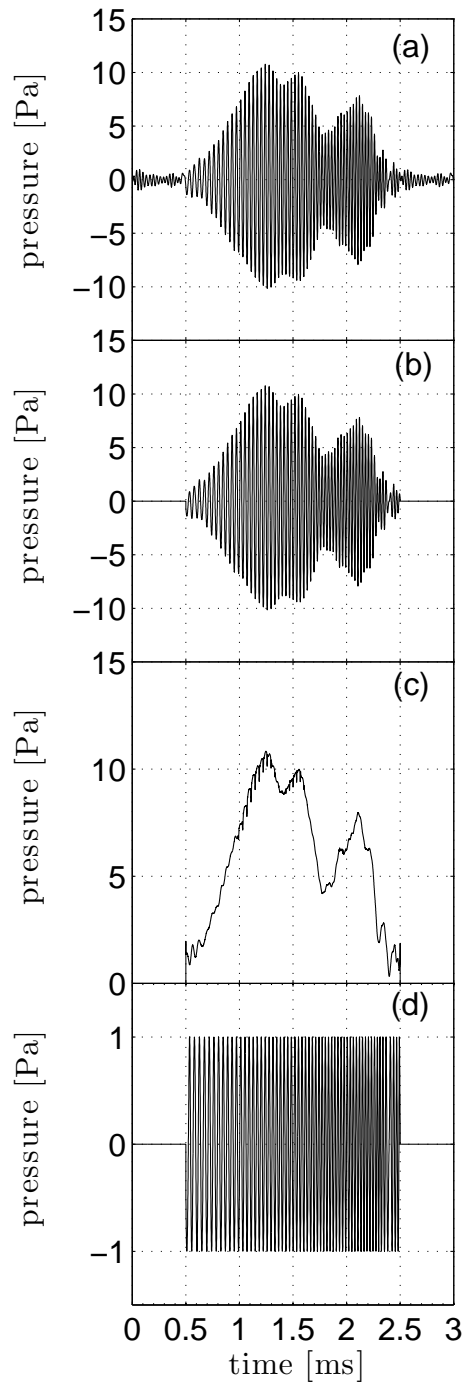


Figure 8: Pre-processing of signal measured by M1. (a) high pass filtered signal; (b) output of the multiplication between the filtered signal and the rectangular box function; (c) envelope of the signal; (d) normalized signal.

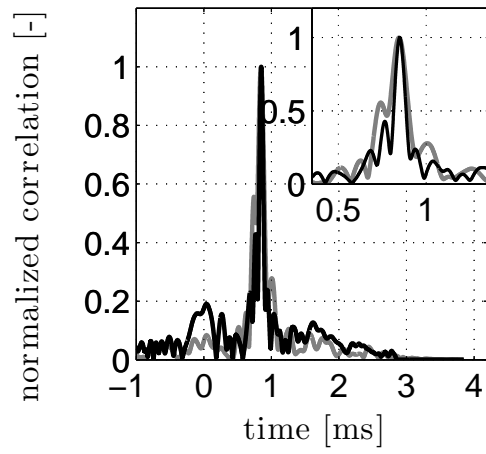
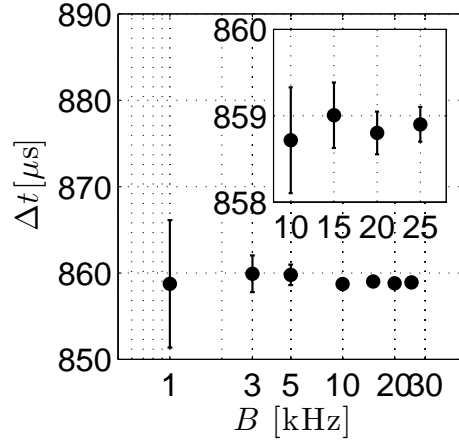
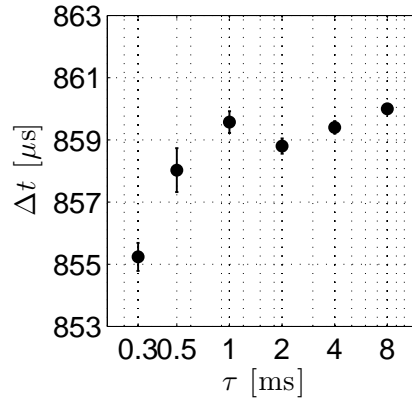


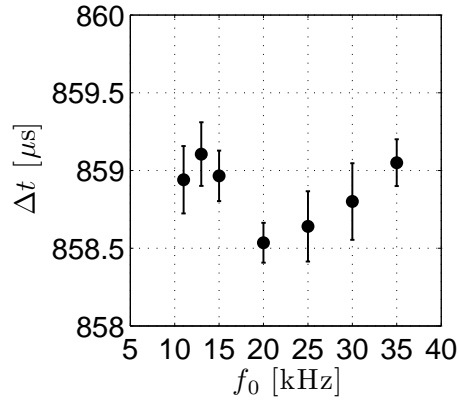
Figure 9: Comparison of the cross-correlations with (black line) and without pre-processing (gray line).



(a) Effect of B .



(b) Effect of τ .



(c) Effect of f_0 .

Figure 10: Effects of the chirp parameters on the determination of the sound travel time Δt . See Tab. 1 for values of the remaining parameters. The distance between the transmitter and receiver is $L = 300$ mm. The speed of sound at ambient conditions is $c_o = 348$ m.s $^{-1}$. Theoretically, the sound travel time is $\Delta t_{th} = 860$ μs in this case.

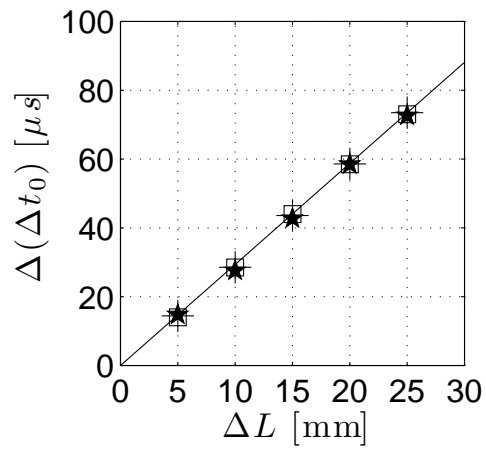


Figure 11: Evolution of the sound travel time difference $\Delta(\Delta t_0) = \Delta t_0(L) - \Delta t_0(L_0)$ with the distance $\Delta L = L - L_0$. The solid line indicates theoretical predictions deduced from Eq. (1). Markers denote measures in the absence of burner (\square), with burner ($+$), and for a non-reacting jet flow ($*$).

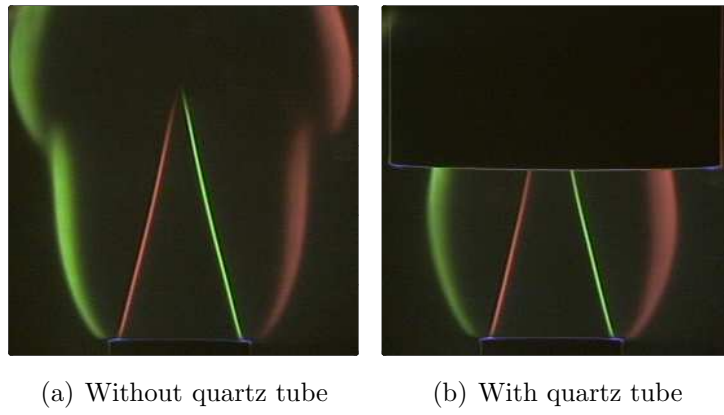


Figure 12: Color Schlieren images of a methane-air premixed flame ($\phi = 0.90$, $v_u = 1.50$ m.s⁻¹) with and without quartz tube on the top of the flame.

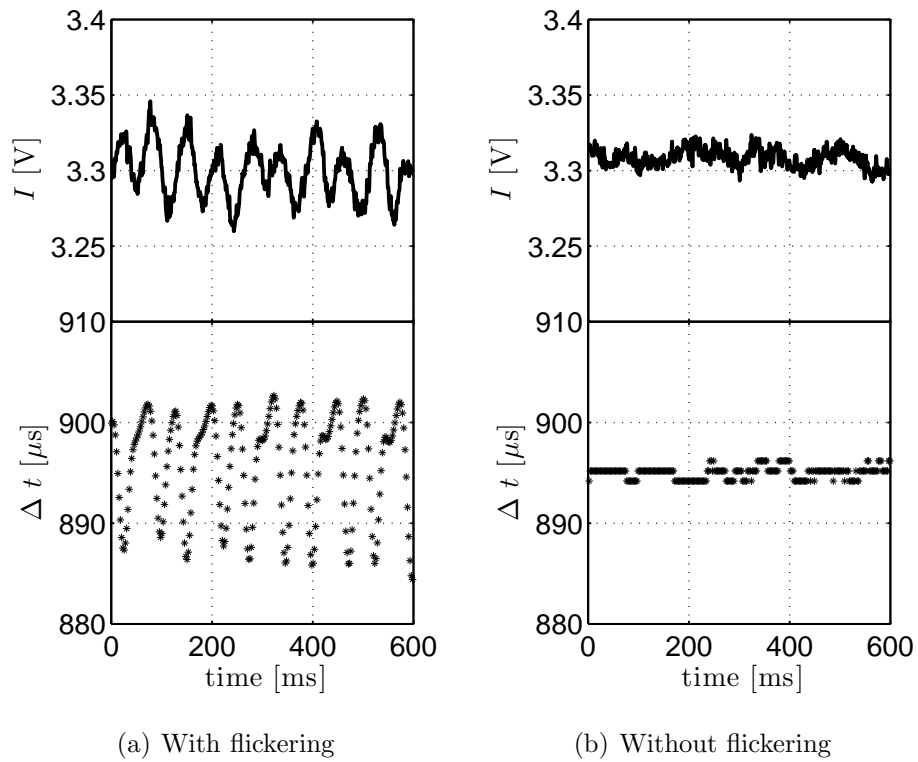


Figure 13: Light emission (top) and sound propagation time (bottom) across a methane-air premixed flame ($\phi = 0.90$, $v_u = 1.50 \text{ m.s}^{-1}$) with and without flickering.

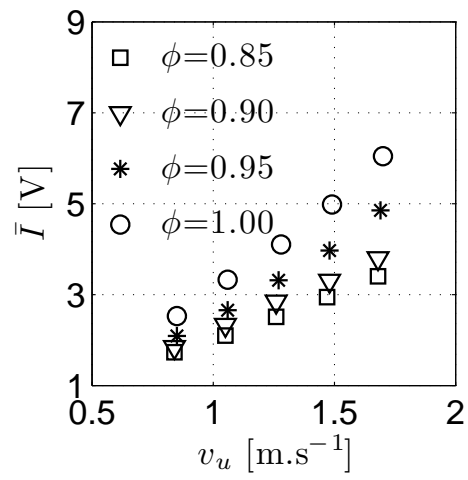


Figure 14: Evolution of the mean flame emission intensity \bar{I} as a function of the flow velocity v_u for different equivalence ratios ϕ .

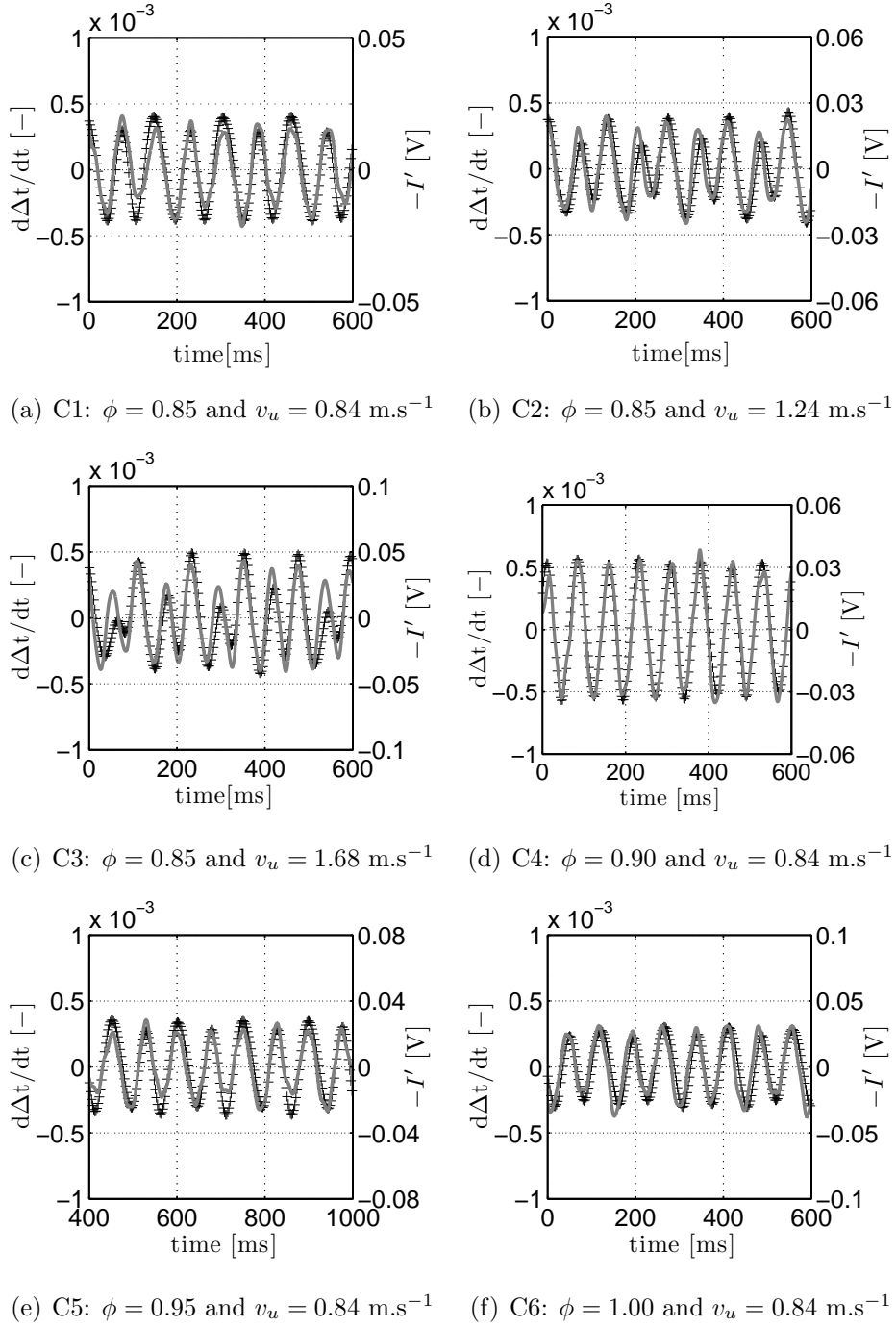


Figure 15: Simultaneous records of chemiluminescence intensity perturbations $-I'$ (solid line) and disturbances in the rate of change of the sound travel $d\Delta t/dt$ (+).

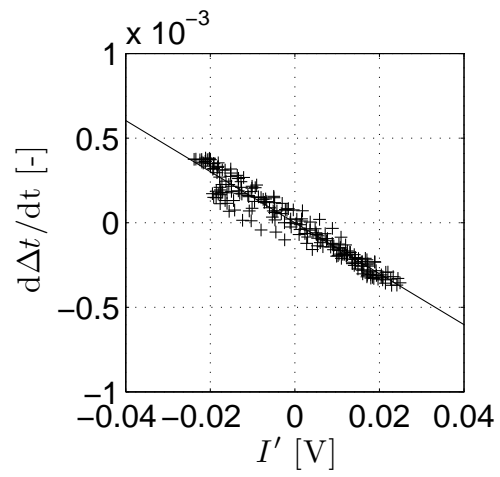


Figure 16: Plot of the rate of change of travel time of ultrasonic waves $d\Delta t/dt$ versus light intensity fluctuations of the flames I' . Flame C2: $\phi = 0.85$ and $v_u = 1.24 \text{ m.s}^{-1}$.

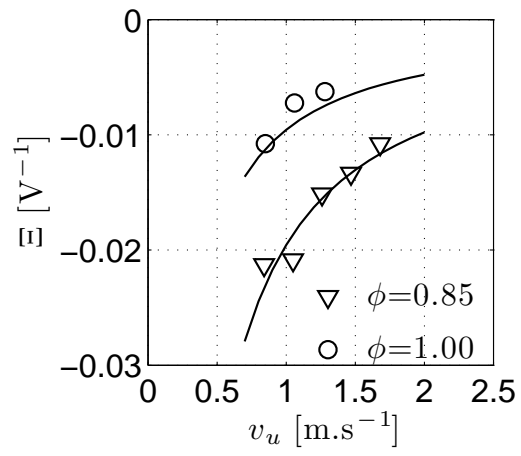


Figure 17: Comparison between measurements and predictions (solid line) for the coefficient Ξ for two equivalence ratios $\phi = 0.85$ (∇) and $\phi = 1.0$ (\circ) as function of the flow velocity v_u .

666 **List of Tables**

667	1	Configurations tested for the chirp generation.	53
668	2	Optimized values for the chirp parameters.	54
669	3	Inlet flow velocity v_u and equivalence ratio ϕ used for the six	
670		configurations explored (Ci). The measured value of the co-	
671		efficient Ξ is also indicated together with the corresponding	
672		value of the linear regression factor r^2	55
673	4	Numerical values used to estimate the coefficient Ξ appearing	
674		in Eq. (16).	56

Table 1: Configurations tested for the chirp generation.

Case	B [kHz]	τ [ms]	f_0 [kHz]
Effect of B	1- 25	2	30
Effect of τ	20	0.3 - 8	30
Effect of f_0	20	2	11 - 35

Table 2: Optimized values for the chirp parameters.

B [kHz]	τ [ms]	f_i [kHz]	τ_r [ms]
20	2	20	2.5

Table 3: Inlet flow velocity v_u and equivalence ratio ϕ used for the six configurations explored (Ci). The measured value of the coefficient Ξ is also indicated together with the corresponding value of the linear regression factor r^2 .

Case	C1	C2	C3	C4	C5	C6
ϕ	0.85	0.85	0.85	0.90	0.95	1.0
v_u [m.s ⁻¹]	0.84	1.24	1.68	0.84	0.84	0.84
Ξ [V ⁻¹]	-0.0213	-0.0151	-0.0108	-0.0137	0.0125	-0.0107
r^2	0.88	0.93	0.81	0.95	0.87	0.92

Table 4: Numerical values used to estimate the coefficient Ξ appearing in Eq. (16).

ϕ	S_L [m.s ⁻¹]	c_u [m.s ⁻¹]	c_b [m.s ⁻¹]	Δq [kJ.kg ⁻¹]	ϵ [V.s.m ⁻¹]	α
0.85	0.31	343	797	1740	1.99	0.1
1.00	0.38	343	834	1930	4.08	0.1